

A new concept of (open) TE₀₁₁ cylindrical cavity

G. Annino[@], M. Cassettari, and M. Martinelli

Istituto per i Processi Chimico-Fisici, CNR, via G. Moruzzi 1, 56124 Pisa (Italy)

(Dated: March 20, 2006)

Abstract

The confinement properties of the open structure formed crossing a circular waveguide perpendicular to a parallel-plate waveguide are discussed, highlighting the fundamental differences with respect to the common high-frequency resonators. Among the electromagnetic modes trapped at the intersection region of the two waveguides, the TE₀₁₁ one appears as the most appropriate for high-frequency applications. Its characteristics are investigated in detail, calculating the mode chart and the related quality factor and power-to-field conversion efficiency. The mode chart is then determined for configurations including a sample holder, in which one of the component waveguides is filled with a low-loss dielectric material. The TE₀₁₁ mode reveals, in particular, remarkable merit figures, as well as a significant stability with respect to the geometrical imperfections and to the insertion of a sample holder. The obtained results show that the proposed single-mode resonator can compete with the standard cavities in terms of performance, versatility, and simplicity.

[@] e-mail address: geannino@ipcf.cnr.it

1. Introduction

The millimeter wave region of the electromagnetic spectrum knew in the last years a rapidly growing activity, following the improved accessibility to these wavelengths guaranteed by the developments in source and detector technology. A relevant effort was in particular dedicated to the realization of the basic passive components of a typical spectroscopic setup, as low-loss waveguides [1], polarizers [1, 2], non-reciprocal elements [3], and resonators [4-6]. In the last case, the solutions commonly adopted at millimeter wavelengths are borrowed from the adjacent spectral regions, where the technology of the resonant cavities is well established. The main challenge in the development of resonators is the realization of a device combining the performances of the single-mode cavities, typically employed at microwaves, with the versatility of the overmoded Fabry-Perot resonators, mainly employed at far infrared and higher frequencies. On the other hand, such device should not present the counterpart of the above benefits, namely the mechanical complexity of single-mode cavities and the extended volume of Fabry-Perot, which often represent a limitation for millimeter wave applications.

It has been recently demonstrated that a system of coupled waveguides shows a variety of electromagnetic modes trapped at their intersection region [7-17]. Such system can behave as a single-mode resonator which combines a very simplified spectrum to high performances, according to the preliminary analysis of Ref. [18]. Among the proposed geometries, the intersection of a cylindrical waveguide with a parallel-plate waveguide appears as the most appropriate for practical applications, in virtue of its largely open structure and to the presence of transverse electric (TE) modes. The trapping of electromagnetic radiation at the intersection of the waveguides is in general due to a proper combination of symmetry of the configuration and cutoff frequency of the modes propagating along the waveguides. Such mechanism of confinement is rather dissimilar from that of a close metallic box resonator, based on a complete shielding of the radiation, as well as from that of the Fabry-Perot, explainable in terms of a simple geometrical optics representation. The confinement of electromagnetic radiation at the intersection of coupled waveguides lead therefore to a new conception of open resonator, the design and the operation of which requires a dedicated approach.

The aim of this article is a systematic investigation of the properties of the TE_{011} mode trapped at the intersection between a cylindrical waveguide and a parallel-plate waveguide. Such investigation will be based on the numerical modelling of the essential parameters of the mode. It will be in particular determined the mode chart, the quality factor and the power-to-field conversion efficiency obtainable in the allowed configurations. The mode chart will then be determined for practical working configurations in which a dielectric sample holder is inserted in the resonator. The obtained results will show that the proposed open single-mode resonator represents a favourable synthesis of ease of realization, open structure, and high performances, which prefigures its employment in demanding applications.

2. Theoretical and experimental background

The demonstration of the existence of electromagnetic (e.m.) modes trapped at the intersection region of coupled metallic waveguides represents a relatively recent achievement. The first results, based on the TE modes of crossed rectangular waveguides [13-17], have been generalized to the hybrid modes of configurations with different waveguides [18], and to configurations including dielectric regions [19].

The common aspect of such systems is the existence of confined solutions with frequency below and above the cutoff of the modes propagating along the waveguides. The basic reason that ensures the confinement of the radiation is the availability, at the intersection region, of a volume with minimum linear size larger than that available in each individual waveguide [11].

In virtue of the enlarged volume, some electromagnetic modes can exist at frequencies lower than the lowest cutoff of the propagating modes. Such isolated modes are necessarily confined because, in the limit of infinite waveguides, they do not have any channel to decay. On the other hand, some confined solutions can exist above the lowest cutoff of the crossed waveguides. Such modes are embedded in the continuous spectrum of propagating modes, which therefore represent possible leakage channels. The additional mechanism that forbids the radiation leakage is in general given by the symmetry of the configuration, which introduces selection rules for the coupling of the confined modes to the propagating ones. It follows, accordingly, that the symmetry plays a basic role in the definition of the confinement properties of coupled waveguides. On the basis of its analysis, for instance, the minimum frequency interval in which a mode with a given symmetry can be trapped is easily predictable [18].

In the idealized condition of perfect conductors, exact geometry and infinite waveguides, the trapped modes appear as resonances with infinite quality factor. In any practical case, the imperfect geometry and the finite conductivity and length of the employed waveguides limit the figure of merit of the resonant device. Nevertheless, the quality factor achievable in the presence of the ohmic losses alone can be quite high, also at millimeter wavelengths. Analogously, the violation of the symmetry due to the geometrical imperfections introduces in general marginal losses at the level of fabrication tolerances which is typical of these wavelengths [18]. The unloaded merit factor Q_0 of such a resonator can be therefore quite high. Its excitation requires a coupling between the electromagnetic energy stored in the intersection region and that propagating in external guiding systems. The coupling can be obtained employing waveguides with finite length. Such operation introduces, as usual, a certain level of irradiation losses. However, being the excitation enhanced by the resonance effect, the coupling level necessary to reach a complete transfer of energy to the high Q_0 resonances can be quite low. As a consequence, the excitation setup is expected to introduce a weak perturbation on the field distribution of these modes.

In one of its simplest form, a coupled-waveguide resonator is realized intersecting a circular waveguide with a parallel-plate waveguide having parallel axis of symmetry [18, 19]. The resulting structure is shown in Fig. 1, together with a possible excitation configuration in which the incoming radiation is coupled to the resonance mode through the parallel-plate waveguide [19]. Alternatively, the excitation can be obtained by coupling the radiation through the circular waveguide, as experimentally verified. In both schemes, the resonance can be detected by monitoring the reflected signal.

When compared with the common millimeter wave resonators, the structure of Fig. 1 certainly shows a surprising topology. Contrarily to the case of close metallic cavities, the radiation stored in the intersection region can escape both radially and axially, through large apertures which minimum size is comparable with that of the confinement region. The proposed resonator can be seen as a cylindrical metallic cavity in which the plungers are removed and the body (the remaining cylindrical waveguide) is cut in two parts. It is worth emphasizing that the cut in the body of the cavity is essential to obtain the trapping of some modes, since the simple cavity without plungers cannot basically resonate. The additional aperture in the open cylinder ensures the confinement of the radiation, instead to introduce a further leakage, as suggested by the common sense. On the other hand, such resonator is still more dissimilar to the open Fabry-Perot cavity. In the case of the Fabry-Perot, indeed, the confinement of the radiation is guaranteed by the concavity of the (real or fictitious) mirrors, which refocuses the radiation on each reflection on them. Here, the metallic surface is neither simply concave nor convex. The profile of such surface - with its sharp edges directed towards the storing region - would suggest the escape of the radiation, instead of its confinement. Nevertheless, it is possible to conclude that, in a sense, the edges help in taking in place the

radiation [9]. The apparent paradox holds only in the geometrical optics representation, which is not applicable here due to the closeness between the size of the confinement region and the employed wavelength. A correct explanation of the confinement mechanism requires in fact a pure wave analysis.

The proposed resonator cannot be classified, therefore, in none of the common classes of resonant structures. Looking at the possible roots of the proposed device, an evident analogy can be established with the nonradiative dielectric resonator discussed in Ref. [19], in the limit of unitary permittivity of the dielectric waveguide. The resulting structure can be equally seen as a generalization of the open nonradiative cavity proposed in Ref. [20].

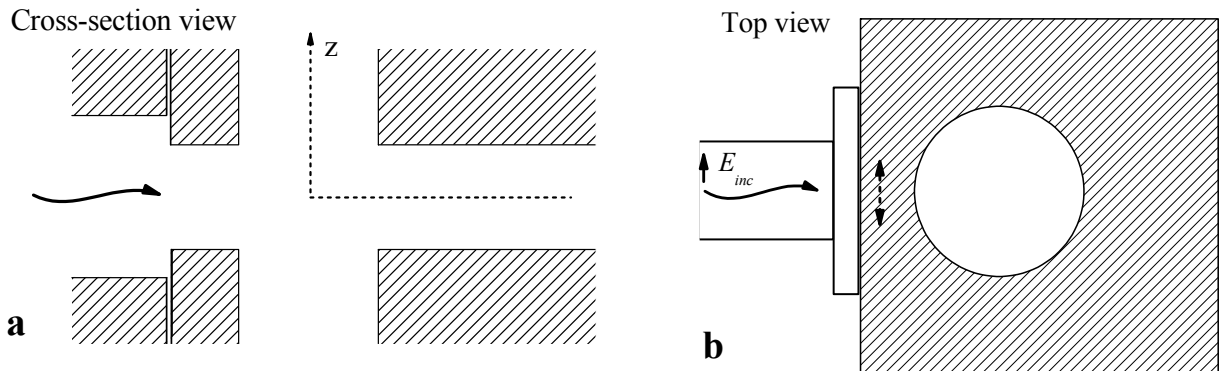


Fig. 1. Sketch of the resonant device obtained coupling a circular waveguide to a parallel-plate waveguide, together with the excitation setup. **a)** Cross-section view. The dashed lines delimit the quarter of the axial cross section on which the e.m. field are calculated (see text). **b)** Top view. The incoming radiation is linearly polarized along the parallel plates. The coupling level is adjusted moving the resonant assembly as indicated by the dashed arrows. The undulated arrows indicate the incoming radiation.

The spectrum of the coupled-waveguide resonators is composed by few resonances determined by the geometry of the configuration, in which the field distribution typically extends over about a wavelength [18]. The structures with rotational invariance show some peculiar characteristics. They are in general compatible with transverse electric (TE) and transverse magnetic (TM) modes with null azimuthal index (vanishing derivative along the azimuthal coordinate), as demonstrated in Appendix (see also Ref. 21). A confined TE_{011} mode has been experimentally observed in various open structures with such symmetry [18, 19, 22]. The research presented in the following will focus on this mode, which is of remarkable importance in practical applications [4, 23-28].

Fig. 2 shows the typical absorption curve of the TE_{011} mode, observed in the configuration of Fig. 1. In such measurement, the resonator was composed by two square plates of anticorrosive alloy with 6 mm thickness and 16 mm side, kept at a distance of 1.7 ± 0.05 mm. The diameter of the hole representing the circular waveguide was 4.1 ± 0.05 mm, and the distance between the hole and the closest lateral edge 1.4 ± 0.05 mm. The curve of Fig. 2 is normalized to the incident power, by dividing the signal obtained with the excitation waveguide close to the intersection region to that obtained far from it [19]. Despite the simplicity of the structure, the unloaded merit factor of the TE_{011} mode reaches the value of $Q_0 = 2400$. The measured resonance frequency, $\nu_0 = 81.44$ GHz, can be compared with the theoretical value of 81.6 ± 1.5 GHz, calculated by means of the finite-element software Multiphysics 3.2a (COMSOL, Sweden) neglecting the excitation setup. The uncertainty in the calculated frequency is determined by the fabrication tolerances. The good agreement with the measured value

confirms the weak perturbation introduced by the excitation setup. A similar result follows from the numerical analysis of the complete configuration. The electric field distribution of the TE_{011} mode on the axial cross section of the cavity is shown in the inset of Fig. 2. Such distribution is plot only on a quarter of the cross section, in virtue of the azimuthal invariance of the mode and of the mirror symmetry of the structure with respect to the median plane of the parallel plates. The condition of radial confinement of the TE_{011} mode follows directly from its field structure. As shown in Appendix, indeed, it does not share any field component with the cutoff-less transverse electromagnetic modes (TEM) propagating along the parallel-plate waveguide. Accordingly, the radial leakage vanishes provided that $l < \frac{\lambda_0}{2}$, being in turn $l = \frac{\lambda_0}{2}$ the first cutoff condition of the parallel-plate TE modes. Here λ_0 is the resonant free-space wavelength. The axial confinement is ensured when λ_0 satisfies the condition $\frac{r}{\lambda_0} < \frac{3.8317}{2\pi}$, where $\frac{r}{\lambda_0} = \frac{3.8317}{2\pi}$ is the first cutoff of the TE_0 modes propagating along the circular waveguide [19].

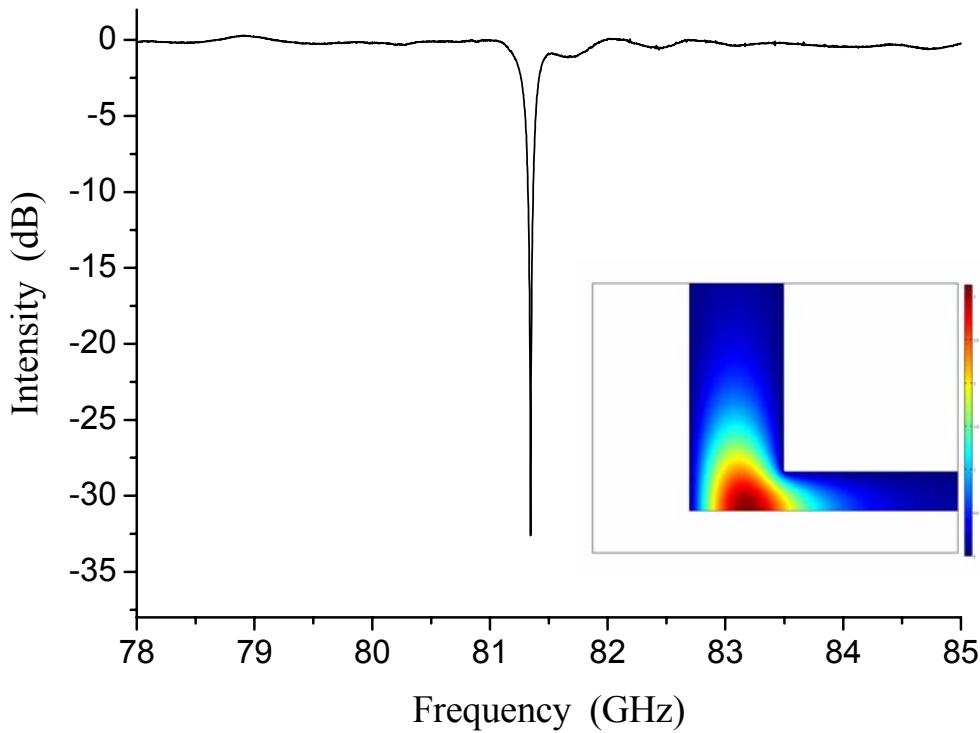


Fig. 2. Normalized absorption spectrum of the TE_{011} mode. Inset: calculated electric field distribution on a quarter of the axial cross section of the resonator. On the right, the colors (gray) scale, expressed in arbitrary units.

3. Mode chart

A complete information on the possible geometry of a resonant device, and on its relation with the frequency of a specific mode, can be encoded in a single graph, namely in the mode chart of the device. The mode chart of the TE_{011} mode is reported in Fig. 3, in terms of the radius r of the cylindrical waveguide and of the distance l between the parallel plates, both

normalized to λ_0 . In order to avoid the divergence of the e.m. field at the sharp edges delimiting the intersection region, the edges were replaced by a circular profile with radius of curvature $\frac{\rho}{\lambda_0} = 25 \cdot 10^{-3}$.

The insets of Fig. 3 show the field distribution of the TE_{011} mode, calculated for the limit conditions indicated by the two external dashed arrows. The solid arrow in the middle of the curve indicates the configuration to which refers the field distribution of Fig. 2. The functional relationship $\frac{r}{\lambda_0} \left(\frac{l}{\lambda_0} \right)$ inside the interval of modelling, $\frac{l}{\lambda_0} \in (0.18, 0.497)$, can be reproduced very accurately by a 9th degree polynomial curve $\frac{r}{\lambda_0} = \sum_{j=0}^9 a_j \left(\frac{l}{\lambda_0} \right)^j$. The values of the coefficients a_j are reported in the Table. Such polynomial function generates the fitting curve of Fig. 3. The relationship between r and l is monotonic; such property allows obtaining the resonance frequency of an arbitrary geometry.

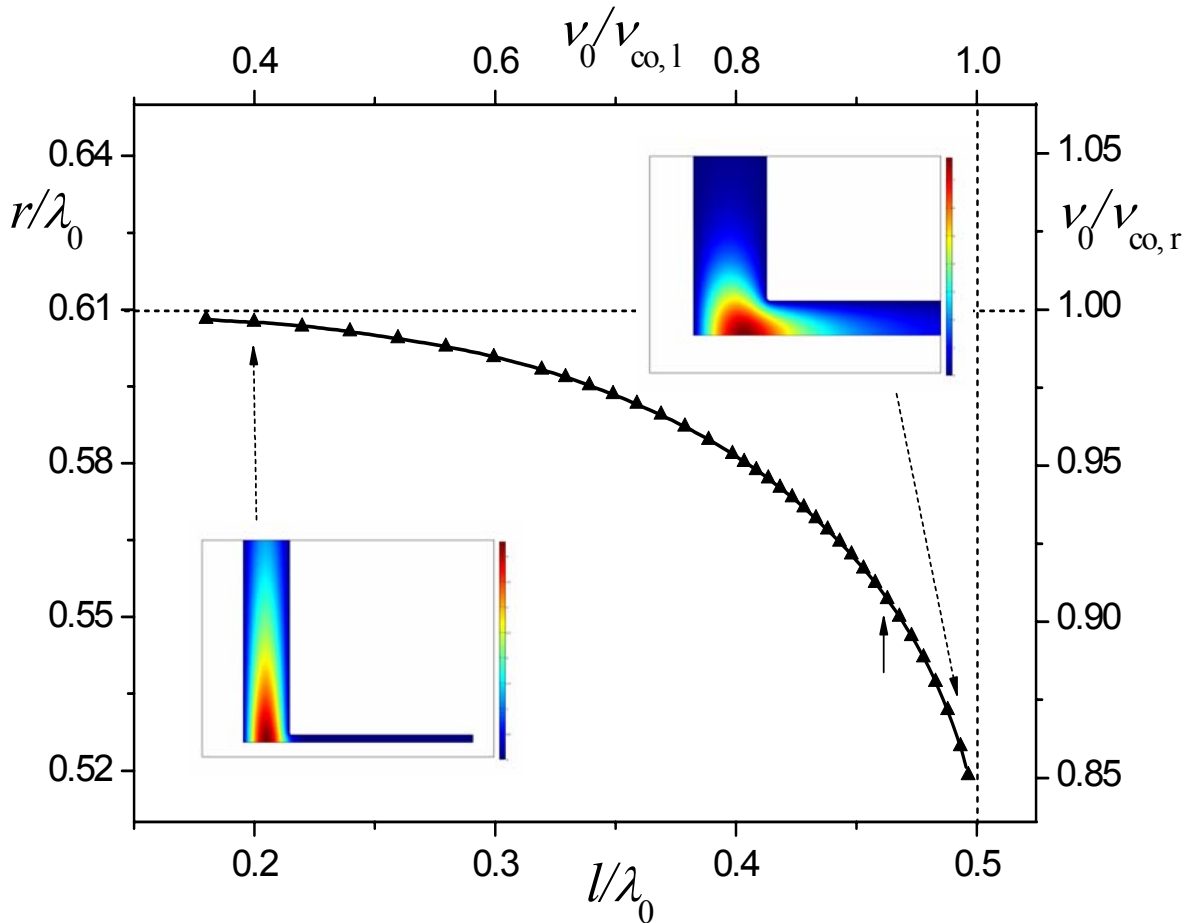


Fig. 3. Mode chart of the TE_{011} mode (see text for the meaning of the labels). The up triangles represent the calculated values, the solid line the fitting curve. The horizontal and vertical dashed lines indicate the theoretical asymptotes. Insets: electric field distribution corresponding to the geometry indicated by the dashed arrows. On the right, the colors (gray) scale, expressed in arbitrary units. The solid arrow indicates the configuration considered in Fig. 2.

In the central part of the $\frac{r}{\lambda_0}$ vs. $\frac{l}{\lambda_0}$ curve, the electromagnetic energy outside the intersection region is almost equally distributed between the cylindrical waveguide and the parallel-plate waveguide. Moving away from this condition, the curve shows an asymptotic convergence in both directions, towards the points $\frac{l}{\lambda_0} = a_1$ and $\frac{r}{\lambda_0} = a_2$. The two asymptotes a_1 and a_2 correspond very well with the theoretical values $a_1 = \frac{1}{2}$ and $a_2 = \frac{3.8317}{2\pi}$, indicated in Fig. 3 by the dashed lines. In the limit in which one of the two variables $\frac{r}{\lambda_0}$ and $\frac{l}{\lambda_0}$ tends to its asymptotic value, the other tends to zero. The field distribution becomes accordingly more and more extended along one waveguide, and only marginally extended in the other. Nevertheless, the narrow waveguide is still capable to induce a trapping of the radiation in the intersection region. This is true, in principle, for any finite size of such guide, at least in the limit of perfectly conducting walls [29, 30]. However, when the secondary guide is very narrow, the mode is so extended along the main one that it cannot be trapped in structures with reasonable size. In the case of Fig. 3, the calculation has been stopped when the relative difference between the variable and its expected asymptote was lower than 1%. The confinement level of the mode can also be evaluated comparing its resonance frequency with the cutoff frequencies of the intersecting waveguides. The relative value of such frequencies is indicated in the right coordinate axis and in the up abscissa axis of Fig. 3. Here, ν_0 is the resonance frequency, $\nu_{co,l}$ the first cutoff of the TE modes of the parallel-plate waveguide, $\nu_{co,r}$ the first cutoff of the TE₀ modes of the circular waveguide.

Table Coefficients of the 9th degree polynomial function fitting the mode chart curve. The standard deviation of the fit is $1.06 \cdot 10^{-4}$.

a_0	17.64
a_1	-522.62
a_2	7021
a_3	-54208.7
a_4	265156
a_5	-852422
a_6	1.80184E6
a_7	-2.4161E6
a_8	1.86592E6
a_9	-632737

According to the mode chart of Fig. 3, the TE₀₁₁ mode exists for a wide range of geometrical conditions. Its practical applicability is strictly related to the figure of merit of the resonance, which is usually expressed in terms of the unloaded quality factor Q_0 and of the power-to-field conversion efficiency. The latter figure gives the root mean square of the electric or magnetic field at a specific point of the resonator, for unitary dissipated power P . The quality factor is important in any application related to the capability of the device to discriminate in frequency, as in the case of frequency filters [31], or when the key parameter is the total

amount of energy stored in the resonator, as for the laser sources [32]. The conversion factor is important when the figure of merit is related to the amplitude of the field inside the resonator. This is the case, for instance, of the absolute sensitivity in electron paramagnetic resonance, related to the magnetic induction field $\bar{B} = \sqrt{\langle B^2 \rangle}$ [33], or to the quantum electrodynamics applications, related to the electric field $\bar{E} = \sqrt{\langle E^2 \rangle}$ [34]. The brackets in the above expressions indicate the average over the oscillation period of the radiation. In the following, the emphasis will be put on the behaviour of the magnetic field \bar{B} ; similar results were obtained, however, for the electric field.

4. Performances

For a copper cavity resonating at 300 GHz, the calculated quality factor Q_0 and axial conversion factor \bar{B}_z (on the point of highest magnetic field) are shown in Fig. 4. The maximum values of these quantities are $Q_0 = 4930$ and $\bar{B}_z = 36.9 \text{ G/W}^{1/2}$; the latter figure is obtained for $\frac{l}{\lambda_0} = 0.39$ and $\frac{r}{\lambda_0} = 0.587$, to which corresponds $Q_0 = 4080$. These figures depend on the radius of curvature of the profile which joins the intersecting waveguides. In particular, at $\frac{\rho}{\lambda_0} = 100 \cdot 10^{-3}$ the maximum quality factor and conversion factor are $Q_0 = 4900$ and $\bar{B}_z = 38.8 \text{ G/W}^{1/2}$, the latter value being obtained for $Q_0 = 4410$ at $\frac{l}{\lambda_0} = 0.357$ and

$\frac{r}{\lambda_0} = 0.579$. Such values can be compared with those of a close cylindrical cavity made with

the same material and resonating at the same frequency. The TE_{011} mode of a cylindrical cavity shows indeed a field distribution similar to that of the mode here investigated; it represents therefore a natural term of comparison for the expected performances. The quality factor and the conversion factor calculated for a copper cavity with optimal aspect ratio are $Q_{0,c} = 5450$ and $\bar{B}_{z,c} = 46.3 \text{ G/W}^{1/2}$.

In the absence of other sources of loss and assuming the resistivity of the conducting walls independent on the frequency ω , Q_0 and \bar{B} follow the simple scaling laws $Q_0 \propto \omega^{-1/2}$ and

$\bar{B} \propto \omega^{3/4}$. Such relations can be deduced from the expressions $Q_0 = \frac{2 \int_{vol} H^2 dV}{\delta \int_{sur} H_t^2 dS}$ [35] and

$\bar{B} = \sqrt{\langle B^2 \rangle} \propto \sqrt{\frac{W}{V}} = \sqrt{\frac{Q_0 \cdot P}{\omega_0 \cdot V}}$ [33]. Here δ is the skin depth in the conductor, H the magnetic

field, H_t its component tangential to the conducting surface, W the total e.m. energy stored in the cavity, V its active volume [36], and ω_0 the angular resonance frequency. Similar relations can be obtained for the dependence of the quality factor and of the conversion factor on the resistivity. In the limit of validity of the perturbative approach, in which the finite resistivity does not appreciably influence the e.m. field distribution, the scaling laws are given by $Q_0 \propto \rho^{-1/2}$ and $\bar{B} \propto \rho^{-1/4}$. Hence, the curves of Fig. 4 can be employed for any resistivity, geometry and frequency.

According to the above analysis, the performances of the proposed open resonator are competitive with those of a standard close cavity. The axial conversion factor \bar{B}_z reaches its maximum value near the center of the mode chart, where the energy of the electromagnetic field shows the minimum spatial spreading. Close to the asymptotes, on the other hand, the active volume of the resonator is so large that the energy density goes to zero, as well as \bar{B} . On the contrary, the merit factor Q_0 shows a monotonic trend and its maximum value corresponds to the minimum allowed distance between the parallel metallic plates. This property suggests that a thin cut orthogonal to a long circular waveguide can trap a TE₀₁₁ mode with high Q value. In this case the electromagnetic energy is widely distributed along the circular waveguide, as shown in the inset of Fig. 3. Nevertheless, the ability of such configuration to discriminate in frequency can be remarkable. A small irregularity in straight waveguides can therefore introduce a sharp behaviour close to the cutoff, as anticipated.

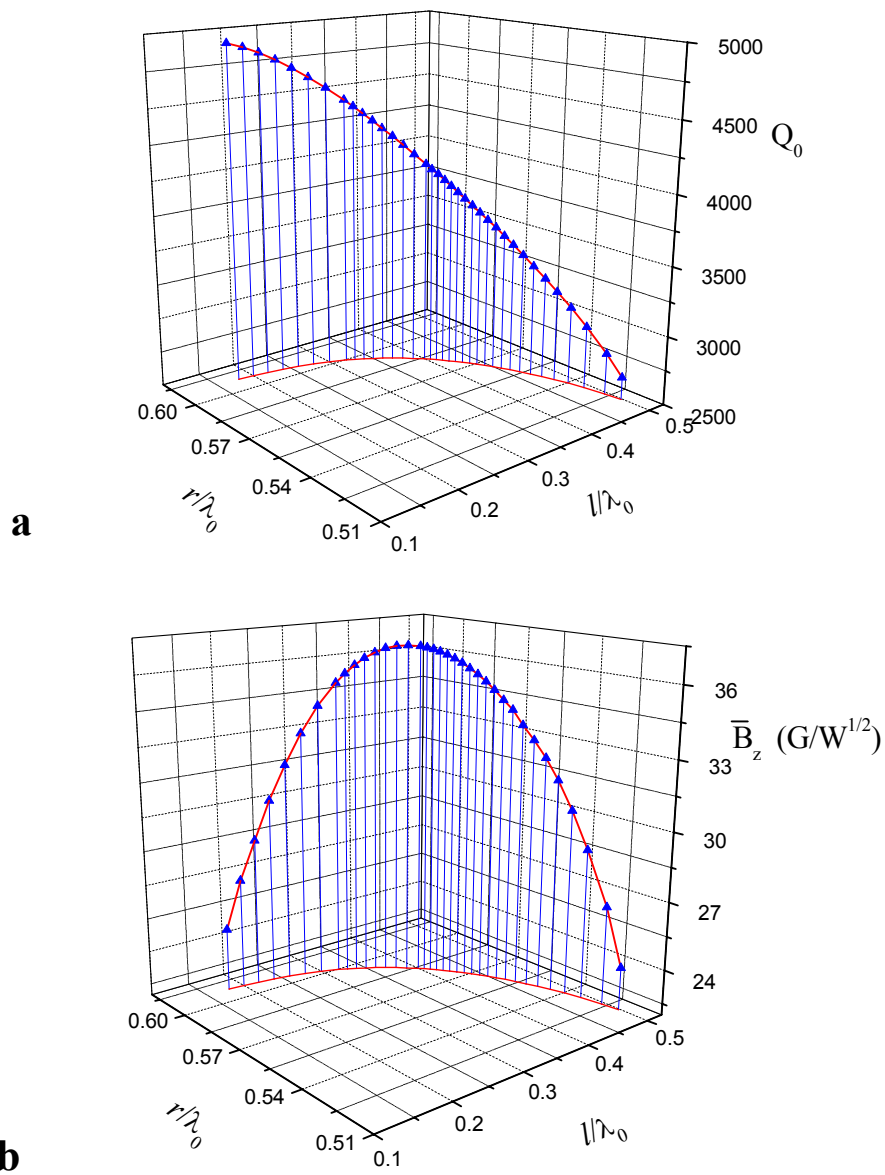


Fig. 4. Calculated merit figures of a room temperature copper (resistivity $1.724 \mu\Omega \text{ cm}$) resonator working at 300 GHz, as a function of the geometry. Blue up triangles: calculated points. Red solid lines: fitting curve. The red solid lines in the r/l planes represent the mode chart curve. **a)** Unloaded quality factor. **b)** Axial magnetic field conversion factor in the center of the resonator.

5. Loaded resonator

In the common spectroscopic applications, it is necessary to introduce a sample in the cavity and very often also a sample holder. In view of a general use of the coupled-waveguide resonator, it is therefore mandatory to evaluate the effects of a low-loss sample holder on its mode chart. Two illustrative cases have been considered: in the first one, the cylindrical waveguide is filled with a dielectric tube made of teflon (dielectric permittivity $\varepsilon = 2.05$); in the second one, a teflon slab is introduced between the metallic plates. Both configurations can be easily realized, in virtue of the open structure of the resonator. The resulting mode charts of the TE_{011} mode are reported in Fig. 5. The limit conditions for such configurations can be predicted following the same approach employed for the analysis of the empty resonator, taking now into account the effective optical size due to the dielectric material. In the case of cylindrical waveguide filled with a medium with permittivity ε , the asymptotes become $\frac{l}{\lambda_0} = \frac{1}{2}$, and $\frac{r}{\lambda_0} = \frac{3.8317}{2\pi\sqrt{\varepsilon}}$ [19].

When the parallel-plate waveguide is filled with a dielectric slab, the asymptotes are $\frac{l}{\lambda_0} = \frac{1}{2\sqrt{\varepsilon}}$, and $\frac{r}{\lambda_0} = \frac{3.8317}{2\pi}$. These limit conditions are well confirmed by the modelling. Similar results have been obtained for other representative cases covering a large interval of dielectric permittivity. Accordingly, the TE_{011} resonance is in general stable with respect to the insertion of a dielectric material along the intersecting waveguides.

From a practical point of view, another basic issue is the tuning of the resonance frequency. In the proposed resonator it can be implemented, for instance, varying the distance l between the parallel plates. The dependence of the resonance frequency on l for a given radius r can be extracted from the mode chart of Fig. 3.

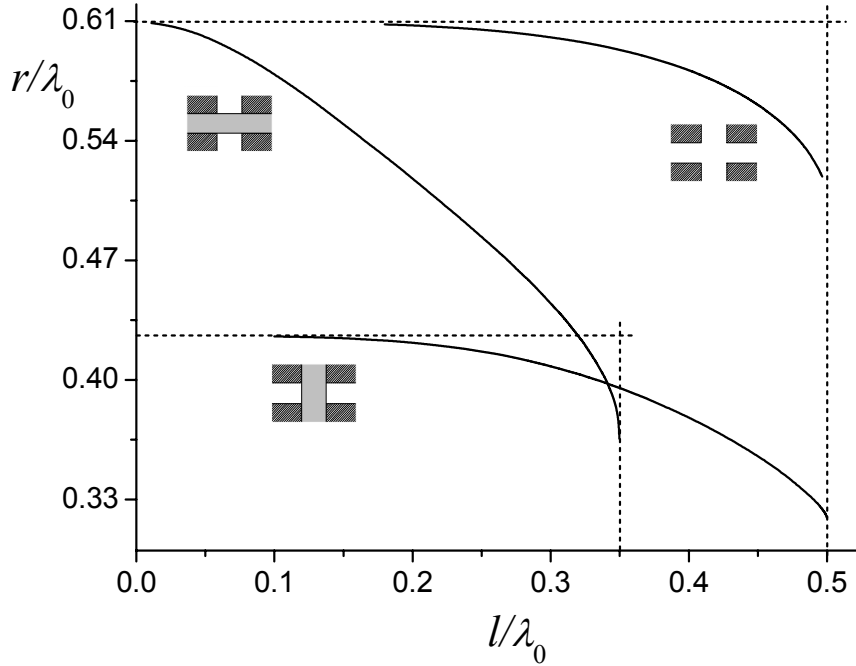


Fig. 5. Mode chart of the TE_{011} mode for different coupled-waveguide structures. The insets sketch the axial cross section of each of them. Top-right: empty resonator. Top-left: Teflon slab filling the parallel-plate waveguide. Bottom-left: Teflon tube filling the circular waveguide. The horizontal and vertical dashed lines indicate the theoretical asymptotes of the different configurations.

In conclusion, the resonator obtained coupling a circular waveguide to a parallel-plate waveguide shows different peculiarities. It combines a largely open structure to a reduced active volume, properties that represent the basis of its simplified spectrum of trapped modes. Among such modes, the TE_{011} one ensures high performances and a weak dependence on the perturbation of the symmetry, without structural degeneracy with other confined modes. It is moreover stable with respect to the insertion of a sample holder along both the component waveguides. The capability of coupled waveguides to trap electromagnetic modes at their intersection region enables, therefore, the realization of a simple and robust resonant device.

Appendix

The vector properties of the electromagnetic modes of a generic system with rotational invariance are considered first, assuming the azimuthal invariance ($\frac{\partial}{\partial\varphi} \equiv 0$) of the solution. A system with no source terms (free charges and currents) and media with finite conductivity will be assumed. Under these assumptions, the conductivity can be included in the complex permittivity.

In a linear and local medium with rotational invariance about the z-direction, the most general expressions for the tensor of the dielectric permittivity and for that of the magnetic permeability are

$$\begin{pmatrix} \varepsilon_{\perp} & 0 & 0 \\ 0 & \varepsilon_{\perp} & 0 \\ 0 & 0 & \varepsilon_z \end{pmatrix}, \quad \begin{pmatrix} \mu_{\perp} & 0 & 0 \\ 0 & \mu_{\perp} & 0 \\ 0 & 0 & \mu_z \end{pmatrix}.$$

In any homogeneous region of this medium, the Maxwell equations can be written in terms of two independent components. Choosing the axial fields as independent fields, the curl equations can be expressed in cylindrical coordinates as [37]

$$\begin{aligned} \left(\frac{\partial^2}{\partial z^2} + \frac{\omega^2}{c^2} \varepsilon_{\perp} \mu_{\perp} \right) H_{\rho} &= j \frac{\omega \varepsilon_{\perp}}{c} \frac{1}{\rho} \frac{\partial E_z}{\partial \varphi} + \frac{\partial^2 H_z}{\partial z \partial \rho}, \\ \left(\frac{\partial^2}{\partial z^2} + \frac{\omega^2}{c^2} \varepsilon_{\perp} \mu_{\perp} \right) E_{\rho} &= \frac{\partial^2 E_z}{\partial z \partial \rho} - j \frac{\omega \mu_{\perp}}{c} \frac{1}{\rho} \frac{\partial H_z}{\partial \varphi}, \\ \left(\frac{\partial^2}{\partial z^2} + \frac{\omega^2}{c^2} \varepsilon_{\perp} \mu_{\perp} \right) H_{\varphi} &= -j \frac{\omega \varepsilon_{\perp}}{c} \frac{\partial E_z}{\partial \rho} + \frac{1}{\rho} \frac{\partial^2 H_z}{\partial z \partial \varphi}, \\ \left(\frac{\partial^2}{\partial z^2} + \frac{\omega^2}{c^2} \varepsilon_{\perp} \mu_{\perp} \right) E_{\varphi} &= \frac{1}{\rho} \frac{\partial^2 E_z}{\partial z \partial \varphi} + j \frac{\omega \mu_{\perp}}{c} \frac{\partial H_z}{\partial \rho}. \end{aligned}$$

In a similar fashion, the divergence equations yield

$$\varepsilon_{\perp} \frac{1}{\rho} \frac{\partial (\rho \cdot E_{\rho})}{\partial \rho} + \varepsilon_{\perp} \frac{1}{\rho} \frac{\partial E_{\varphi}}{\partial \varphi} = -\varepsilon_z \frac{\partial E_z}{\partial z}$$

and

$$\mu_{\perp} \frac{1}{\rho} \frac{\partial(\rho \cdot H_{\rho})}{\partial \rho} + \mu_{\perp} \frac{1}{\rho} \frac{\partial H_{\varphi}}{\partial \varphi} = -\mu_z \frac{\partial H_z}{\partial z}.$$

In the case of solutions with azimuthal invariance, the above equations decouple in two groups, the first one involving the field components $(H_{\rho}, E_{\varphi}, H_z)$ and the second one the components $(E_{\rho}, H_{\varphi}, E_z)$. The former admits therefore TE₀ solutions and the latter TM₀ solutions, which can be in both cases bounded or unbounded. The subscript ‘0’ indicates the azimuthal invariance of the solution. Such two complete sets of modes do not share any field component. However, they can be mixed by the boundary conditions.

Consider now the boundary between two different regions labeled with 1 and 2, and the normal to the separating surface, labeled with \hat{n} . In the above assumptions, the boundary conditions reduce to continuity equations of the form $\begin{Bmatrix} \vec{D}_2 - \vec{D}_1 \\ \vec{B}_2 - \vec{B}_1 \end{Bmatrix} \cdot \hat{n} = 0$ and $\begin{Bmatrix} \vec{E}_2 - \vec{E}_1 \\ \vec{H}_2 - \vec{H}_1 \end{Bmatrix} \times \hat{n} = \vec{0}$.

Where defined, the vector \hat{n} cannot have azimuthal component in virtue of the rotational invariance of the system; consequently, $\hat{n} = n_{\rho} \hat{\rho} + n_z \hat{z}$ at any point. The scalar boundary conditions impose therefore the continuity of the term $\varepsilon_{\perp} E_{\rho} n_{\rho} + \varepsilon_z E_z n_z$ and of the term $\mu_{\perp} H_{\rho} n_{\rho} + \mu_z H_z n_z$, whereas the vector conditions impose the continuity of the components E_{φ} and H_{φ} , and of the terms $n_{\rho} E_z - n_z E_{\rho}$ and $n_{\rho} H_z - n_z H_{\rho}$. Accordingly, also the boundary conditions can be separated in two sets of equations involving the above field components. Since these conditions do not mix the TE₀ and TM₀ partial solutions obtained in each homogenous region, the complete solutions resulting for the whole domain will show the same TE₀ or TM₀ character. The generalization of this result to systems with a continuous variation of permittivity and permeability can be obtained by approximating these quantities with stepwise functions, and then taking the limit. A limit operation on the conductivity of the employed materials can be employed as well to extend the above property to configurations including ideal conductors.

A similar approach can be followed to demonstrate that the modes with azimuthal and axial invariance ($\frac{\partial}{\partial \varphi} \equiv 0, \frac{\partial}{\partial z} \equiv 0$) propagating along a parallel-plate waveguide are, in the limit of ideal conductors, transverse electromagnetic (TEM) with nonvanishing components given by (H_{φ}, E_z) .

References

- [1] P. P. Woskov, V.S. Bajaj, M. K. Hornstein, R. J. Temkin, R. G. Griffin, IEEE Trans. Microwave Theory Tech. **MTT-53**, 1863 (2005)
- [2] D. R. Solli, C. F. McCormick, R. Y. Chiao, J. M. Hickmann, J. Appl. Phys. **93**, 9429 (2003)
- [3] C. R. Boyd, IEEE Trans. Microwave Theory Tech. **MTT-53**, 2371 (2005)
- [4] H. Blok, J. A. J. M. Disselhorst, H. van der Meer, S. B. Orlinskii, and J. Schmidt, J. Magn. Reson. **173**, 49 (2005);
- [5] A. I. Meshkov, F. C. De Lucia, Rev. Sci. Instrum. **76**, 083103 (2005)
- [6] E. M. Ganapolskii, A. V. Golik, A. P. Koroljuk, Phys. Rev. B **51**, 11962 (1995)
- [7] F. M. Peeters, Superlattices and Microstructures **6**, 217 (1989)

- [8] P. Exner, Phys. Lett. A **141**, 213 (1989)
- [9] R. L. Schult, D. G. Ravenhall, and H. W. Wyld, Phys. Rev. B **39**, R5476 (1989)
- [10] P. Exner, P. Seba, and P. Stovicek, Phys. Lett. A **150**, 179 (1990)
- [11] Y. Avishai, D. Bessis, B. G. Giraud, and G. Mantica, Phys. Rev. B **44**, 8028 (1991)
- [12] P. Exner and P. Seba, J. Math. Phys. **30**, 2574 (1989)
- [13] P. Exner and P. Seba, Phys. Lett. A **144**, 347 (1990)
- [14] J. Goldstone and R. L. Jaffe, Phys. Rev. B **45**, 14100 (1992)
- [15] J. P. Carini, J. T. Londergan, K. Mullen, and D. P. Murdock, Phys. Rev. B **46**, 15538 (1992)
- [16] J. P. Carini, J. T. Londergan, K. Mullen, and D. P. Murdock, Phys. Rev. B **48**, 4503 (1993)
- [17] J. P. Carini, J. T. Londergan, D. P. Murdock, D. Trinkle, and C. S. Yung, Phys. Rev. B **55**, 9842 (1997)
- [18] G. Annino, H. Yashiro, M. Cassettari, M. Martinelli, Phys. Rev. B **73**, 125308 (2006)
- [19] G. Annino, M. Cassettari, M. Martinelli, Rev. Sci. Instrum. **76**, 084702 (2005)
- [20] G. Annino, M. Cassettari and M. Martinelli, Rev. Sci. Instrum. **76**, 064702 (2005)
- [21] G. Annino, M. Cassettari and M. Martinelli, <http://ArXiv.org/physics/0408130> (2004)
- [22] G. Annino, M. Cassettari, M. Fittipaldi, M. Martinelli, J. Magn. Reson. **176**, 37 (2005)
- [23] W. Lawson, J. Cheng, J. P. Calame, M. Castle, B. Hogan, V. L. Granatstein, M. Reiser, G. P. Saraph, Phys. Rev. Lett. **81**, 3030 (1998)
- [24] Z. Zhai, C. Kusko, N. Hakim, S. Sridhar, A. Revcolevschi, A. Vietkine, Rev. Sci. Instrum. **71**, 3151 (2000)
- [25] S. S. Chauhan, C. C. Rajyaguru, H. Ito, N. Yugami, Y. Nishida, T. Yoshida, Rev. Sci. Instrum. **72**, 4344 (2001)
- [26] E. Gaganidze, R. Heidinger, J. Halbritter, A. Shevchun, M. Trunin, H. Schneidewind, J. Appl. Phys. **93**, 4049 (2003)
- [27] J. Kim, K. Lee, B. Friedman, D. Cha, Appl. Phys. Lett. **83**, 1032 (2003)
- [28] T. P. Crowley, E. A. Donley, T. P. Heavner, Rev. Sci. Instrum. **75**, 2575 (2004)
- [29] G. V. Stupakov, S. S. Kurennoy, Phys. Rev. E **49**, 794 (1994)
- [30] S. S. Kurennoy, Phys. Rev. E **51**, 2498 (1995)
- [31] L. Z. Duan, K. Gibble, Opt. Lett. **30**, 3317 (2005)
- [32] A. Corney, *Atomic and laser spectroscopy*, (Oxford University Press, Oxford, 1988), chapt. 12 and 13
- [33] C. P. Poole, *Electron Spin Resonance: a Comprehensive Treatise on Experimental Techniques* (Wiley, New York, 1983).
- [34] S. M. Spillane, T. J. Kippenberg, K. J. Vahala, K. W. Goh, E. Wilcut, H. J. Kimble, Phys. Rev. A **71**, 013817 (2005)
- [35] H. A. Atwater, *Introduction to Microwave Theory* (McGraw-Hill, New York, 1962)
- [36] J. T. Robinson, C. Manolatu, L. Chen, M. Lipson, Phys. Rev. Lett. vol. 95, 143901 (2005)
- [37] D. Kajfez and P. Guillon, *Dielectric Resonators* (Artech House, Dedham, 1986)